Vibration and diffusion of Cs atoms on Cu(001)

2007 J. Phys.: Condens. Matter 19 305010

(http://iopscience.iop.org/0953-8984/19/30/305010)

IOP PUBLISHING JOURNAL OF PHYSICS: CONDENSED MATTER

J. Phys.: Condens. Matter **19** (2007) 305010 (18pp) doi:10.1088/0953-8984/19/30/305010

Vibration and diffusion of Cs atoms on Cu(001)

A P Jardine, G Alexandrowicz, H Hedgeland, R D Diehl[1], W Allison and J Ellis

Cavendish Laboratory, J J Thomson Avenue, University of Cambridge CB3 0HE, UK

E-mail: apj24@cam.ac.uk

Received 5 February 2007, in final form 21 March 2007
Published 13 July 2007
Online at stacks.iop.org/JPhysCM/19/305010

Abstract

^{3}He spin-echo (^{3}HeSE) dynamics measurements of low coverages of Cs on Cu(001) both reveal quasi-elastic broadening of the helium beam due to aperiodic transport on the surface, and extend measurements of the previously observed low energy acoustic phonon mode, at coverages between 0.014 and 0.056 ML and temperatures of 130 and 80 K. The low energy phonons and quasi-elastic broadening occur on similar timescales and we separate the contributions by converting the spin-echo measurement to the energy domain. Langevin molecular dynamics simulations reproduce the variation of the quasi-elastic peak width, phonon position and amplitudes with momentum transfer, temperature and coverage. The main features in the experimental data require a potential corrugation of 20 ± 2 meV and a friction parameter of $1/40$ ps^{-1}. Our results indicate that the Cs dynamics are dominated by dipole–dipole repulsion and produce strongly correlated motion. However, contrary to previous expectations the transport proceeds through jump like behaviour within the Cs overlayer, and Cs moves much more freely than other alkali metals on copper. The unusual behaviour that we see requires three critical components; strong interadsorbate forces, a weak but finite substrate corrugation, and low adsorbate–substrate friction. Together, these key features manifest themselves as a distinct signature in the intensity distribution across the energy/momentum exchange spectrum.

(Some figures in this article are in colour only in the electronic version)

1. Introduction

The adsorption of alkali metals on metal surfaces has been studied for more than 80 years [1], and it provided the basis for some of the earliest models of chemisorption [2]. The interest was maintained through the years largely due to the potential for technological applications based

[1] Permanent address: Department of Physics, Penn State University, University Park, PA 16802, USA.

on the ability of alkali adatoms to alter the electronic and chemical properties of surfaces. With the advent of modern surface science techniques, fundamental studies of the structures, electronics and dynamics of alkali metal adsorption systems were carried out as early as the 1960s, but the level of activity increased markedly in the 1990s due to several experimental discoveries, which further motivated the application of modern *ab initio* calculations to these systems. The experimental discoveries were of the 'unexpected' variety, and included the observation of the intermixing of alkali metal atoms with the substrate [3], the observation of stable low coordination alkali adsorption sites [4, 5], and the observation of condensation of the alkali adatoms into dense 2D phases at relatively low coverages [6]. All three of these phenomena were observed on Al surfaces, which stimulated and facilitated the application of density functional theory (DFT) since only 'simple' metals were involved. The theoretical studies provided both an explanation for the unexpected observations and a new paradigm for alkali metal adsorption [7–10].

The picture that emerged included a significant degree of charge transfer, or polarization, of the alkali adatoms at very low coverages leading to dispersed structures, depolarization of the adatoms as the coverage increases and the average adatom separation decreases, and the possibility for condensation when the attractive metallic bonding of the adatoms overcomes the dipole–dipole repulsion. Essentially all of the studies of structures, vibrations and electronics of alkali metals adsorbed on metals were found to fit within this general picture of alkali metal adsorption [11, 12].

Experiments during the past 10 years on the dynamics (vibrations and diffusion) of alkali metals on metal surfaces have provided ever more precise measures of the alkali adsorption forces and interactions that are broadly consistent with the picture described above [13]. However, they also indicate a range of unexpected new phenomena. For instance, a recent study of the diffusion of Na atoms on Cu(001) indicates that in addition to the usual 2D motion in the surface plane, at coverages higher than 0.05 ML an additional small but significant component of confined aperiodic motion appears in the direction perpendicular to the surface [14]. Analysis suggested that as the local Na density increases, the Na atoms, as seen by the helium beam, move away from the surface by ∼0.2 Å. Fluctuations in local density therefore give rise to a hopping like behaviour, but in the direction perpendicular to the surface. This result is surprising since previous experimental and theoretical studies for adsorbed alkalis have shown that the perpendicular spacing for alkali metals is largely independent of coverage, adsorption site and temperature [12]. The current paper applies the same helium spin-echo technique to investigate the dynamics of the Cs/Cu(001) system, which is the alkali metal system that we expect to exhibit the most different behaviour from the now well studied Na/Cu(001) system.

2. Previous studies of Cs on Cu(001)

An early LEED study of Cs on Cu(001) [15] found that at 150 K, the diffraction pattern at low coverages consists of rings, which increase in diameter continuously with coverage until they begin to coalesce into spots at about 70% of the saturation coverage. The rings are interpreted as arising from Cs atoms that are dispersed across the surface, with the average nearest-neighbour distance inversely proportional to the square root of the coverage. The saturation coverage at 150 K corresponds to 0.31 Cs atoms per surface Cu atom. The diffraction spots at 70% saturation (0.22 coverage) correspond to two perpendicular domains of a hexagonal unit cell having a nearest-neighbour spacing of 5.77 Å. As the coverage is increased, it compresses uniformly until a Cs–Cs distance of 5.10 Å. This distance corresponds to twice the Cu lattice spacing in the ⟨110⟩ direction, and a further increase in coverage results in a uniaxial compression of the lattice in the perpendicular direction, creating a quasi-hexagonal unit cell.

The Cs lattice compresses continuously as the coverage is increased until it reaches a Cs–Cs distance of 4.84 Å in the non-commensurate direction. A spot profile analysis (SPA) LEED study at 120 K found the same behaviour [16]. The situation is similar for adsorption at room temperature, with the onset of the ordered structure occurring at somewhat higher coverage and the saturation coverage being somewhat lower [15].

More recent x-ray diffraction studies were performed at room temperature to elucidate the lateral order and adsorption geometries [17, 18]. The truncation rod analysis was interpreted to indicate multiple site occupation at the lowest coverages. The structure was found to be quasi-hexagonal for the saturated monolayer, in agreement with the LEED, and the Cs–Cu average perpendicular spacing was measured to be 2.94 Å [17]. No lateral density modulation of the Cs layer was observed. The thermal disorder was also studied using x-ray diffraction [19]. The diffraction intensities were better fitted by an anharmonic potential model, which was also anisotropic, with mean square parallel vibration amplitudes smaller in the close-packed directions. At 190 K the fitted mean square vibration was 0.07 Å^2 along the commensurate direction and 0.22 Å^2 along the perpendicular direction. At 303 K, the vibrations were found to be more isotropic, attributed to the proximity of the disordering transition ($T = 328$ K) of the Cs structure and the same mean square amplitudes were 0.41 and 0.44 Å^2, respectively.

Two earlier He-atom scattering (HAS) studies of Cs on Cu(001) explored the structural and vibrational properties in the low coverage [20] and monolayer regimes [21]. For coverages below half of a saturated layer, isotropic diffraction rings were observed [20]. The smallest ring corresponded to a Cs–Cs spacing of about 35 Å, indicating strong Cs–Cs repulsion acting over large distances. A vibrational study was carried out at a coverage of 0.08, which corresponds to a Cs–Cs distance of 9.5 Å (the metallic Cs–Cs bond length is 5.46 Å). A low energy surface parallel vibrational mode was measured for momentum transfers $0.1\ \text{Å}^{-1} < \Delta K < 0.4\ \text{Å}^{-1}$ and a weak dispersion was noted. The force constant deduced from this mode ($k_{\mathrm{B}}T \equiv \omega_T/M$) is about 14 meV Å^{-2}, much smaller than corresponding adsorbate–substrate force constants deduced for Na and K [20]. A simple mean field theory was used to model the dispersion relationship, which indicated that the lateral variation in the Cs–Cu(001) potential was close to zero, since the mode energy appears to vanish at $\Delta K = 0$. The friction force was derived from the phonon frequency using the elastic continuum theory [22], giving a relaxation time of 4 ns [20]. In the same study, no quasi-elastic broadening was observed.

The second HAS study was carried out for a full monolayer of Cs [21]. No non-specular diffraction peaks were observed even with a 10^6 sensitivity range, indicative of a very smooth He–Cs potential. Three vibrational modes were observed, identified as substrate Rayleigh and overlayer longitudinal and perpendicular modes. Although the monolayer structure is commensurate in one direction, no gap was observed at the zone boundary of the longitudinal mode, suggesting a lack of lateral corrugation in the Cs–Cu potential. The perceived lack of corrugation was also given as a cause for the relative high intensity of the longitudinal acoustic mode, which had not been observed for Na or K. The conclusion from this study was that the Cs vibrations are effectively decoupled from the substrate, producing quasi-two-dimensional phonon behaviour.

Figure 1 shows a model for the competition between adsorbate–substrate interactions, defined by a corrugated static potential, and adsorbate–adsorbate interactions modelled by harmonic springs. The previous HAS work on this system pointed towards the extreme limit of this model where the corrugation of the adsorbate–substrate potential is negligible. The same work also indicated an extremely small adsorbate–substrate friction, and very strong dipole–dipole repulsion between Cs atoms. However, the fact that the structure is commensurate in one direction at higher coverages indicates that the substrate lateral forces cannot be zero. The

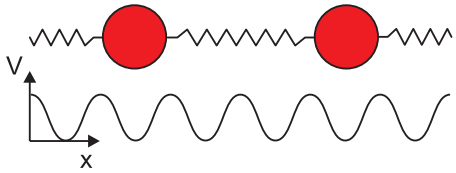

Figure 1. Cartoon illustrating the forces experienced by atoms on a rigid surface. Adsorbate–adsorbate forces are represented by springs, while the adsorbate–substrate forces are represented by a potential energy surface. Typically the adsorbate–substrate forces are dominant (e.g. Na/Cu(001)). For the Cs/Cu(001) system, however, previous work suggests the potential is negligible compared to the strong dipole–dipole repulsion between Cs atoms.

purpose of the present paper is to explain quantitatively the extent to which the uncorrugated substrate model is correct. In fact, we show that although the potential corrugation and friction are weak, they are non-zero, and we establish values for these two parameters. The results confirm that the overlayer dynamics are dominated by adsorbate interactions, but experience an important modulation from the substrate.

3. Experiment

Helium scattering experiments were performed on the Cs/Cu(001) system using the Cambridge ^{3}He spin-echo (^{3}HeSE) instrument [23, 24]. A full description of the measurement principle is beyond the scope of the present article (see [25–27] for more information) and we give only a very brief description of the process here.

Within the beamline of the instrument, which can be considered as an atom interferometer, helium wavepackets are split into two spin components by a magnetic field. These components travel through the machine at different velocities and hence scatter from the sample at different times, separated by an interval t_{SE}, known as the spin-echo time. The scattered components are recombined at the detector and yield a polarization measurement, which corresponds to the autocorrelation of the surface structure as seen by the helium beam. The measurement is sensitive on the timescale t_{SE} (governed by the strength of the magnetic fields used) and in the direction and length determined by the momentum transfer vector $\Delta\mathbf{K}$ (given by the scattering geometry of the measurement). The measured polarization is a complex quantity, as we measure both the amplitude and phase of the recombined beam, and is known as the intermediate scattering function, $I(\Delta\mathbf{K}, t_{\mathrm{SE}})$. The intermediate scattering function is the spatial Fourier transform of the Van Hove pair correlation function, $G(\mathbf{R}, t_{\mathrm{SE}})$, which fully describes the dynamics of the surface [28]. Similarly, $I(\Delta\mathbf{K}, t)$, is the temporal Fourier transform of the dynamic structure factor, $S(\Delta\mathbf{K}, \omega)$, the quantity measured in a conventional energy resolved scattering experiment.

The single-crystal Cu(001) sample was mounted on the instrument sample manipulator, permitting translations, polar and azimuthal rotations, heating and cooling. The manipulator was then installed in the experimental chamber of the spin-echo spectrometer (base pressure $\sim 4 \times 10^{-11}$ mbar after bakeout). The crystal surface was prepared by repeated cycles of sputtering with 800 eV Ar ions and subsequent annealing to 800 K. The quality of the surface was monitored using the specular He reflectivity (typical helium reflectivity was >0.25). Cs was dosed onto the surface from a SAES Getters dispenser, which gave a maximum pressure rise of $\sim 5 \times 10^{-10}$ mbar during deposition. All helium scattering experiments were performed with a beam energy of 10 meV.

The specular intensity variation measured during Cs deposition was very similar to that observed in earlier studies [16, 29]. The coverage for the measurements presented here was

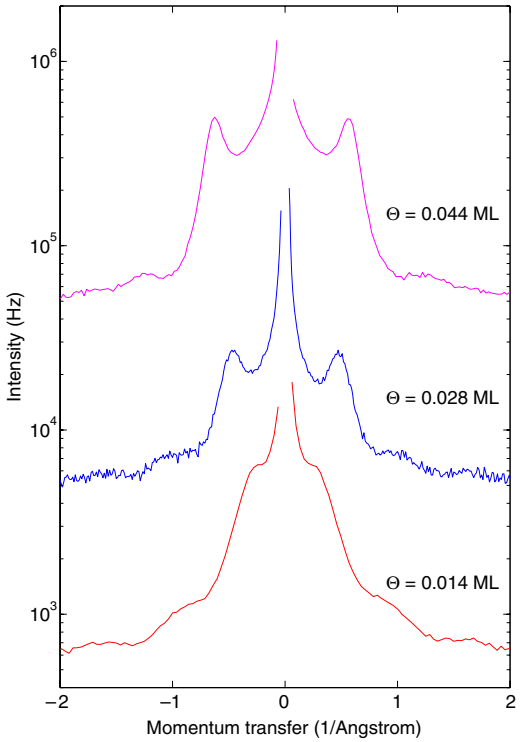

Figure 2. Helium-3 diffraction scans for Cs on Cu(001), along the ⟨100⟩ substrate direction, at coverages of 0.014, 0.028 and 0.044 ML (at temperatures of 130, 130 and 80 K respectively). The total scattering angle and beam energy are fixed at 44.4° and 10 meV respectively, while the angle of incidence is varied in order to obtain the diffraction pattern. The measurements at 0.028 and 0.044 ML are displaced by factors of 10 and 100 respectively. The central peak is due to the specularly reflected beam and is omitted for clarity, as it corresponds to a count rate of several hundred MHz. The first subsidiary peak corresponds to a diffraction ring and does not vary significantly with azimuthal sample orientation, indicating an absence of azimuthal ordering. Several very weak additional peaks are also observed, which we attribute to higher order diffraction rings.

determined from the location of diffraction features. Figure 2 shows three angular scans of the scattered He intensity. The observed off-specular peaks are radial profiles through the isotropic diffraction rings that result from the Cs overlayer that has a well defined nearest-neighbour distance but no long-range orientational order. The radius of the inner ring is related to the average nearest-neighbour distance r by $\mathbf{K}_{\text{ring}} = 4\pi/\sqrt{3}r$ [16]. Weak second- and third-order peaks are evident in the angular scans, which we attribute to higher order diffraction peaks, an indication of a narrow distribution of nearest-neighbour distances.

4. Results

^{3}He spin-echo measurements were made at 130 and 80 K for Cs coverages of between 0.014 and 0.056 ML and for a range of surface parallel momentum transfer values, $\Delta\mathbf{K}$, between $\sim$0.04 Å^{-1} and 1.2 Å^{-1}. The scattered intensity was found to drop off quickly with both increasing $\Delta\mathbf{K}$ and coverage. The effect was more marked than in the Na/Cu(001) system and it limited the range of coverage and momentum transfer that could be measured. In each

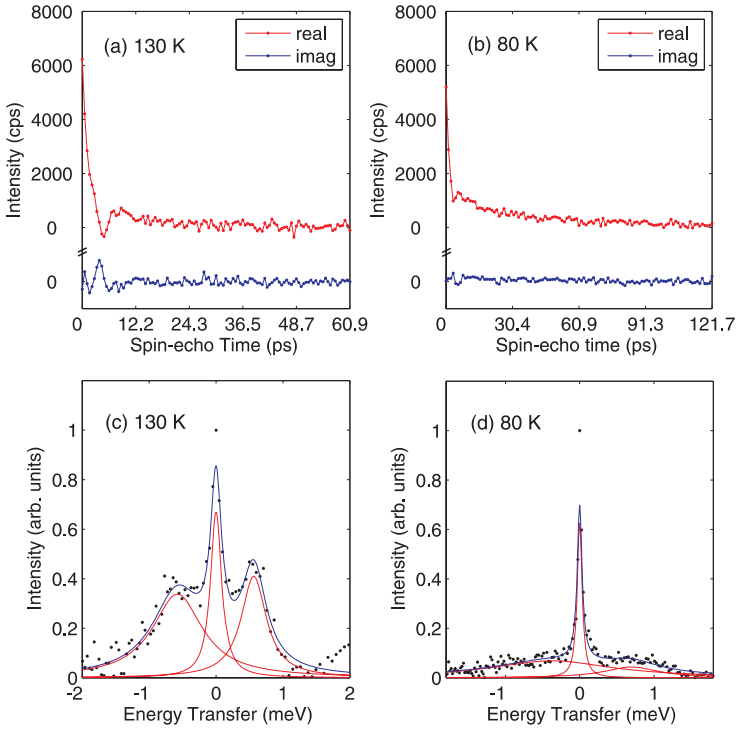

Figure 3. ^{3}He spin-echo measurements performed along the ⟨100⟩ substrate direction for a 0.044 ML coverage of Cs on Cu(001) at (a) 130 K and (b) 80 K (at $\Delta\mathbf{K} = -0.27$ and -0.31 Å^{-1} respectively). The real and imaginary components of the complex polarization are shown separately. The oscillation in (a) corresponds to a phonon mode, while the exponential decay that is present in both (a) and (b) corresponds to a quasi-elastic broadening due to diffusion. A constant background count rate corresponding to the mean count rate of the fully polarized beam has been subtracted from both the real and imaginary parts, and an additional constant count rate has been subtracted from the real component to compensate for the elastically scattered component of the beam. (c) and (d) show the spin-echo time/wavelength Fourier transforms of (a) and (b) after having been converted to an energy transfer scale (note that (a/b) and (c/d) are not direct time–energy transforms). The central quasi-elastic peak is broadened by Cs diffusion, and the phonon modes are now visible as finite energy transfer peaks. The central point is unusually high and indicates imperfect elastic correction in the time domain. The solid lines in (c) and (d) show a Lorentzian fit to the data (excluding the central point), as described in the text.

measurement, both the real and imaginary components of polarization of the scattered beam were measured as a function of spin-echo time. Measuring both of these components enables us to reconstruct the spectra without imposing an artificial symmetry [25].

Typical results are shown in figure 3(a) for a coverage of 0.044 ML and a temperature of 130 K, where the real and imaginary components are shown separately. The overall decay of the real part corresponds to the dephasing of the surface configuration with time, as measured for the particular length scale and direction on the surface. Looking closely, we see that the real component has an oscillation as well as an overall decay, this oscillation can also be seen in the imaginary component. Oscillations in the polarization correspond to atoms on the surface moving with a characteristic period, i.e. to a particular vibrational mode or surface phonon. The decay in the amplitude of this oscillation with spin-echo time reflects the coherency and lifetime of this vibration.

Figure 3(b) shows an equivalent measurement at 80 K. In this case we see the oscillatory phonon amplitude has almost entirely disappeared from the data, leaving an approximately exponentially decaying real part and an almost flat imaginary part. Such a signature indicates aperiodic diffusion on the surface and is equivalent to a quasi-elastic broadening in the energy domain [26]. For simple diffusion processes (e.g. Brownian motion or hopping) the polarization decays exponentially with time and so an exponent can be fitted to the data. The decay constant, which characterizes the process, may be extracted for further analysis. Such curve fitting is the standard approach to interpreting ^{3}HeSE measurements of diffusion[2].

Given we observe diffusion at 80 K, we also expect faster diffusion at 130 K. However, the strong phonon amplitude at 130 K, combined with the fact that phonon and diffusion decays act over similar timescales, makes it difficult to identify and curve fit a distinct decay component for each process. Hence, in order to separate out the different frequency components, we prefer to work in the energy domain. We apply a Fourier transform to the measurement and obtain the dynamic structure factor, $S(\Delta\mathbf{K}, \omega)$. A full description of the transform, which must be applied in wavelength space, is provided in [25].

The resulting energy transfer spectra for the 130 and 80 K measurements are shown in figures 3(c) and (d) respectively, and are analogous to the intensity versus energy spectrum obtained in a time-of-flight (TOF) experiment. The energy resolution is indicated by the spacing of the points in the spectrum and is determined by the largest spin-echo times used in the time domain. We now see distinct quasi-elastic peaks at both temperatures, accompanied by energy loss and gain peaks at 130 K. As in the time domain, the vibrational mode amplitudes at 80 K are much lower, the well defined energy gain and energy loss peaks are replaced by broad, weak peaks and the quasi-elastic peak is significantly narrower, indicating slower diffusion.

4.1. Phonon component

In order to reduce the quantity of data and make possible a comparison with dynamical models, the energy domain spectra have been fitted using three Lorentzian peaks, of variable position, height and width. The mid-point of the central peak is constrained to zero to model the quasi-elastic peak, while the other two peaks are constrained to energy loss and gain appropriately (while also being constrained to avoid the substrate Rayleigh and Longitudinal resonance modes). The fit is applied over the region shown in figures 3(c) and (d) and the results of the fit are shown superimposed on the spectra. The overall procedure provides a remarkably good fit to the data. At 130 K, where the phonons can be clearly resolved, dispersion curves were extracted from the position of the phonon peaks.

Figure 4 shows the dispersion of the phonon energies along the ⟨100⟩ direction at 130 K, for coverages of 0.028, 0.044 and 0.056 ML. The ΔE versus $\Delta\mathbf{K}$ dependence of the phonon energy follows the sinusoidal form for an acoustic mode of the Cs overlayer that was predicted by Senet *et al* [20]. The amplitude of the curves increases with coverage, indicative of an increase of the parallel force constant, as expected, since the dipole interactions increase in this coverage range. The data in figure 4 are matched with a simple sinusoidal form, which we use below in order to refine the fitting process.

Our dispersion curve is in the form of an acoustic mode approaching zero at the zone centre, as has been previously seen by Senet *et al* [20]. In fact, our measurements which follow the mode at lower $\Delta\mathbf{K}$ provide considerably stronger evidence for this observation. Senet *et al* [20] use this observation to infer that the Cs–substrate lateral potential corrugation is negligible. However, as we will discuss below, the low temperature data combined with the quasi-elastic peak measurements lead to a different picture of the surface dynamics.

[2] Usually the amplitude of phonon oscillations is quite small, since the low energy helium beam has a low probability of exciting phonons and the oscillations decay quickly compared to the decay due to diffusion.

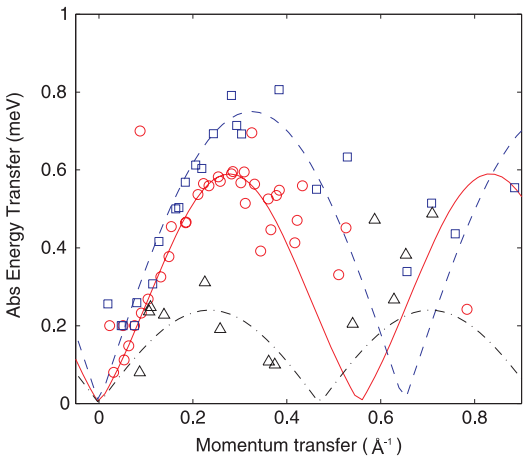

Figure 4. Measured phonon energies for the parallel acoustic mode of Cs on Cu(001). The measurement was carried out along the ⟨100⟩ substrate direction for coverages of 0.028 ML (triangles), 0.044 ML (circles) and 0.056 ML (squares). The phonon positions are obtained from the positions of the relevant peaks that result from the three-Lorentzian fit described in the text. The mode clearly follows a sinusoidal form and approaches zero energy transfer at zero momentum transfer. Above about 0.5 Å^{-1} the phonon amplitudes are very low, and consequently the scatter in these points increases considerably. The lines provide a sinusoidal form to guide the eye.

4.2. Quasi-elastic component

Following the usual approach to quasi-elastic analysis we now examine the variation of the quasi-elastic peak width, ΔE_{QE}, with momentum transfer, adsorbate coverage and surface temperature. The dependence of the quasi-elastic peak width on these parameters reflects both the rate and mechanism of microscopic diffusion [26]. The broadening of the quasi-elastic peak is obtained from a separate fit to the data in which the phonon frequencies are constrained to follow the smooth models shown in figure 4. The process minimizes the number of free parameters in the fit and hence reduces the uncertainty of the extracted quasi-elastic peak broadening. At 80 K, where clear phonons cannot be observed we use the previous procedure.

Figure 5 shows the extracted width of the quasi-elastic peak as a function of $\Delta\mathbf{K}$ for coverages of 0.014 and 0.044 ML and temperatures of 130 and 80 K. From these measurements we can identify several important features. First of all, the magnitude of the quasi-elastic broadening indicates a very high mobility of Cs atoms. In particular, Cs moves more freely than either Na [14, 30] or K on Cu(001) [31], both of which are otherwise considered as moving unusually quickly. For example, the quasi-elastic broadenings measured at 130 K and 0.014 ML correspond to a hopping rate $>$10 GHz. In contrast, in the earlier HAS study of Cs on Cu(001) at low coverage [20], the lack of observation of quasi-elastic broadening led to the conclusion that diffusion is slower compared to other alkali atoms due to the strong interadsorbate forces.

The variation of the quasi-elastic peak width, ΔE_{QE}, with $\Delta\mathbf{K}$ provides much more information, including details of the diffusion mechanism and information about the Cs–Cs interactions. For a simple jump mechanism due to activated jumping of isolated atoms in a corrugated potential, we would expect the peak width to vary sinusoidally with $\Delta\mathbf{K}$, reaching a maximum at the Brillouin zone boundary ($\sim$1.7 Å^{-1} along the ⟨100⟩ direction). In contrast, at the exceptionally low coverage of 0.014 ML (figure 5(a)), where isolated diffusion dominates, the quasi-elastic peak width is rather flat with $\Delta\mathbf{K}$. The flat shape is consistent with a wide distribution of multiple jump lengths (which add a series of higher frequency oscillations into

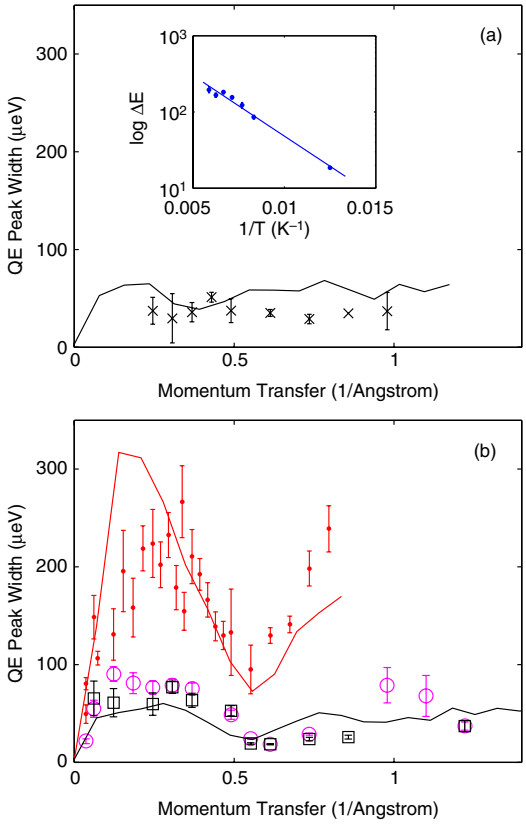

Figure 5. Quasi-elastic peak width (FWHM) as a function of momentum transfer in the ⟨100⟩ substrate direction for (a) 0.014 ML at 130 K (crosses) and (b) 0.044 ML at 130 K (dots) and 0.044 ML at 80 K (circles). (b) also shows the broadening in the ⟨110⟩ direction for 0.044 ML at 80 K (squares). At low coverages the broadening is approximately flat, suggesting Cs atoms move as isolated atoms in a low friction regime. At higher coverages a pronounced peak and dip appear, indicating correlated Cs motion. The low temperature measurements also suggest the dynamics are isotropic. The solid curves are obtained using the MD simulations described in the text. Inset: Arrhenius plot of the quasi-elastic peak width against inverse temperature, measured at 0.044 ML coverage and $\Delta\mathbf{K} = 0.61$ Å^{-1} along the ⟨100⟩ substrate direction. The gradient of the plot gives an effective activation energy of 31 ± 2 meV.

the $\Delta E_{\mathrm{QE}}/\Delta\mathbf{K}$ curve), and typically arises when the friction is very low [33]. There is no direct evidence of Cs–Cs interaction at this coverage (see below). It is also worth noting that the exceptionally large diffuse scattering cross section of helium at isolated adatoms makes such low coverage measurements possible.

As the coverage is increased slightly to 0.044 ML (figure 5(b)), there is a dramatic change in the value and the momentum transfer dependence of the quasi-elastic broadening. The magnitude of the broadening increases quickly with increasing $\Delta\mathbf{K}$, and a pronounced dip develops. Generally speaking, when correlated motion dominates, the quasi-elastic broadening is inversely proportional to the lifetime of a certain surface structure. For an adsorbate system with repulsive lateral interaction, the longest lived structure corresponds to the preferred hexagonal overstructure. Thus at the $\Delta\mathbf{K}$ value which corresponds to the mean Cs–Cs spacing in the hexagonal structure, we expect to see a dip in the quasi-elastic broadening, also known as

a de Gennes narrowing [32]. The de Gennes dip can be seen at $\Delta\mathbf{K} \sim 0.6$ Å^{-1}, which is also the position of the diffraction ring presented earlier. The lifetime of other 'non-preferred' adsorbate structures reduces as the coverage and the corresponding repulsive interaction is increased. Hence, for other $\Delta\mathbf{K}$ values the quasi-elastic broadening increases with coverage, as can be seen in figure 5(b).

In the measurements at 80 K, the quasi-elastic peak is well separated from the phonon modes, hence yielding smaller error bars in the extracted quasi-elastic peak widths and allowing the measurements to be made to larger values of momentum transfer than at 130 K (figure 5(b)). A similar variation of the quasi-elastic peak with momentum transfer is obtained, supporting the conclusions above. Because of the improved data quality, the 80 K measurements were carried out along both the principal substrate directions, ⟨100⟩ and ⟨110⟩. We find very similar results along the two directions, indicating that the diffusion is isotropic.

The inset to figure 5(a) shows an Arrhenius plot of the quasi-elastic broadening at a coverage of 0.044 ML and a momentum transfer of 0.61 Å^{-1}. The plot forms a straight line, indicating activated dynamics with an activation energy of 31 ± 2 meV. This value is much lower than the case of Na, indicating Cs dynamics are much more weakly thermally activated.

4.3. The complete low energy group

Although the fitted data sets allow us to apply conventional analyses to the measurements, it is also possible to combine all experimental data sets to provide an overview of the entire measurement across the low energy 'group'. The transformed experimental data sets can be plotted together to form a 2D plot of intensity as a function of both parallel momentum transfer, $\Delta\mathbf{K}$, and energy transfer, ΔE, i.e. plotting the dynamic structure factor, $S(\Delta\mathbf{K}, \omega)$. Although this technique has been used previously to visualize simulated data [33], this is the first time experimental data have been plotted in this way.

Figure 6 shows such plots for (a) 130 K and (b) 80 K, using colour to represent intensity. As before, we see that at 130 K both the quasi-elastic intensity (energy transfer centreline) and phonon intensities are clearly visible, whereas at 80 K the two phonon peaks disappear leaving only the quasi-elastic component of the spectrum visible. We can also distinguish the variation in the width of the quasi-elastic peak with $\Delta\mathbf{K}$, that the low energy phonon mode appears to cross zero at $\Delta\mathbf{K} = 0$, and that there is a narrowing of the entire data set at about $\Delta\mathbf{K} = 0.6$ Å^{-1}, corresponding to the de Gennes feature described above. The 2D plot at 130 K is characterized by a significant phonon intensity which drops off quite sharply with increasing momentum transfer, at about $\Delta\mathbf{K} = 0.4$ Å^{-1}. In conjunction with the dispersion relationship, the phonon and quasi-elastic peaks form a qualitative 'arrowhead' shape, pointing towards the origin.

The 'arrowhead' shape, which characterizes $S(\Delta\mathbf{K}, \omega)$ at 130 K disappears when the temperature is lowered to 80 K, and also disappears when the coverage is reduced to 0.014 ML. This change is an important guide to the nature of the system, and can be qualitatively explained from the schematic diagram shown in figure 1. If the corrugation is finite, then at low coverage and temperature the adsorbates will be trapped in the adsorption sites and will not move freely within the dipole–dipole mean field, i.e. we will expect a T-mode rather than an acoustic mode. However, increasing either the surface temperature or the coverage (and hence the strength of the dipole–dipole interaction) will facilitate motion out of the adsorption well and enable collective vibrations within the dipole–dipole mean field, giving rise to the 'arrowhead' shape.

In summary, the experimental data on this system are characterized by the two main features. First, an experimental phonon dispersion curve at 130 K which appears to reach the origin, but which broadens and disappears at both low coverage and low temperatures, as

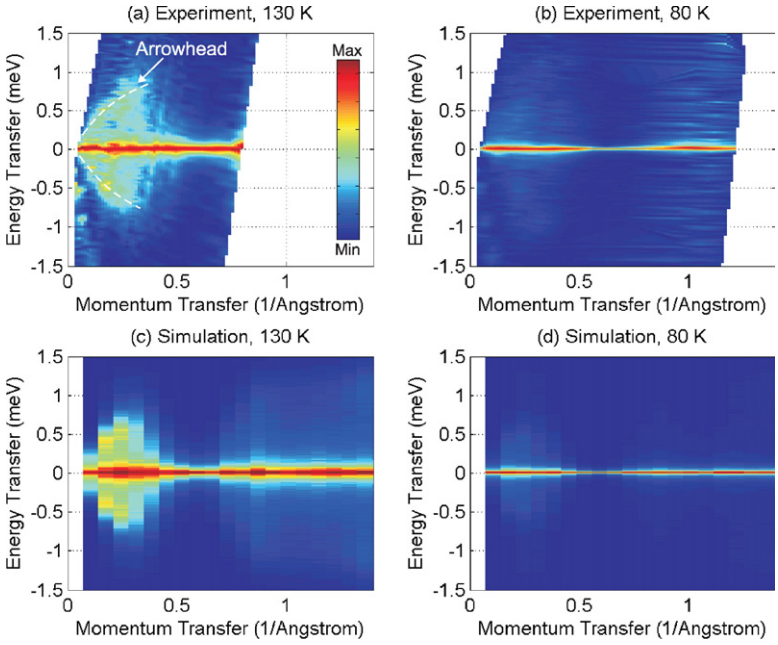

Figure 6. Example two-dimensional plots of intensity against energy and momentum transfer, i.e. $S(\Delta\mathbf{K}, \omega)$, along the $\langle 100 \rangle$ substrate direction, for both experimental and simulated data at a coverage of 0.044 ML. Colour represents intensity as indicated by the bar in (a). (a) and (b) are compiled from experimental data at 130 and 80 K respectively. At 130 K the phonon modes and quasi-elastic peak are clearly visible. Phonon intensity drops away at about 0.4 Å^{-1} and forms a distinctive 'arrowhead' shape which we find is a valuable guide to the behaviour of the system. The phonon modes are almost completely absent at 80 K. The narrow ridge passing through $\Delta\mathbf{K} = 0.05$ Å^{-1}, $\Delta E = -1$ meV is the substrate Rayleigh mode. (c) and (d) show corresponding plots at 130 and 80 K for data generated using the MD simulations described in the text. The 'arrowhead' shape is well reproduced, along with the absence of the phonon modes at low temperature.

discussed above. The second feature is an isotropic quasi-elastic broadening which is roughly constant with $\Delta\mathbf{K}$ at low coverage, suggesting low adsorbate–substrate friction. At higher coverages the variation of the broadening with $\Delta\mathbf{K}$ indicates correlated motion. Similar motion has been seen for Na, but in the case of Cs the motion is much faster and there are much stronger levels of correlation at lower coverages. The coexistence of the periodic and aperiodic motion which give rise to these two features reflects the balance between the adsorbate–adsorbate and adsorbate–substrate coupling in this system, which we examine quantitatively in the next section.

5. Molecular dynamics simulation

We now use Langevin molecular dynamics (MD) and scattering simulations to quantify the deductions from experiment. The MD approach that we use has previously been described in some detail [26, 30] and involves calculating the motion of a collection of Cs atoms as they move over an adiabatic potential energy surface which represents the lateral Cs–Cu forces. The simulations are designed to be as simple as possible, while still reproducing the observed behaviour. Adsorbate coupling to the substrate electron/phonon bath is included through a uniform friction parameter, η, while interadsorbate forces are included directly through an

explicit Cs–Cs interaction. For convenience we also use τ, the time over which the kinetic energy of a particular adsorbate atom remains correlated, where $\tau = 1/\eta$.

Sodium dynamics on Cu(001) have been extensively measured and analysed using this MD technique, and reproduce almost all the dynamical data available [14, 30, 34]. We therefore have adopted similar interaction potentials to use with Cs. For the Cs–substrate interaction we use the first-order sinusoidally corrugated potential defined by bridge and top site barriers to diffusion, E_b and E_t, according to

$$V(x, y) = \frac{E_t}{4} + \frac{E_b}{2} + \frac{E_t}{4}\left[\cos\left(\frac{2\pi x}{a}\right) + \cos\left(\frac{2\pi y}{a}\right)\right] + \frac{1}{4}(E_t - 2E_b)\cos\left(\frac{2\pi x}{a}\right)\cos\left(\frac{2\pi y}{a}\right). \quad (1)$$

Cs–Cs forces are modelled using a dipole–dipole repulsion model [30]. The coverage dependent dipole moment was extracted from work function measurements by Arena *et al* [35], which within the coverage range of this study are well reproduced using a Topping model with a polarizability of 32.5 Å^3 and a zero coverage dipole moment of 7.9 D. Simulations involving 110 atoms were run for a total of 2.1 ns in 10 fs timesteps. Kinematic scattering calculations were performed every 32 timesteps throughout the simulation to generate the intermediate scattering function $I(\Delta\mathbf{K}, t)$. This function was subsequently Fourier transformed to obtain the dynamic structure factor, $S(\Delta\mathbf{K}, \omega)$, which was compared with the reconstructed experimental spectra.

Simulated results of $S(\Delta\mathbf{K}, \omega)$ are shown as two-dimensional colour plots in figures 6(c) and (d). We find that these colour plots provide an excellent guide to the potential and friction parameters that are required to reproduce the experimental data. In particular, we find that reproducing the 'arrowhead' shape requires some quite stringent conditions. We quickly find that Cs requires a much lower lateral substrate corrugation than other alkalis on copper. However, we find that, unlike the predictions from the model in [20], a small but finite corrugation is essential. In fact, to reproduce the form of figure 6(a) we require both a finite but small corrugation and a finite but weak frictional coupling between the Cs atoms and the substrate. Using either a flat substrate potential, regardless of friction, or too high a friction, does not give the characteristic 'arrowhead' that we see experimentally.

In order to perform a detailed comparison, we perform the same triple-Lorentzian fit as was applied to the experimental data. The different measurement coverages enable both the potential and friction to be determined. At 130 K and 0.044 ML coverage the simulated quasi-elastic broadening is relatively insensitive to friction, but the magnitude of the broadening, particularly around the de Gennes features, varies quite strongly with potential corrugation. In contrast, at 130 K and 0.014 ML, where we see the flat curve in the experiment, we find the magnitude of the simulated results varies with both friction and potential. The stronger dependence on friction which arises at low coverage (in the absence of strong Cs–Cs interactions), is consistent with the behaviour normally expected for isolated particles. Thus, as the friction is increased, the results tend towards the sinusoidal variation that characterizes simple jump diffusion, whereas if the friction is reduced, the $\Delta E_\mathrm{QE}/\Delta\mathbf{K}$ results flatten out and reduce in amplitude more and more [33]. Hence, by comparing with simulation at both coverages, we can refine the values for both parameters.

Results for the quasi-elastic peak width are shown with the experimental data in figure 5, and were obtained using the final parameters of $E_b = E_t = 20 \pm 2$ meV and $\tau = 40^{+20}_{-10}$ ps. As expected [20], the friction value we find is very much lower than for other alkalis on copper (larger τ). Our measured friction ($1/40$ ps^{-1}) is however much higher than the value predicted by the elastic continuum theory model ($1/4000$ ps^{-1}) discussed in [20].

The strong drop off in experimental quasi-elastic amplitude with momentum transfer meant that it was not possible to make measurements beyond $\Delta\mathbf{K} = 1.2$ Å^{-1}. Consequently, it is not possible to determine the ratio of the potential barrier heights E_b/E_t along the two principle substrate directions conclusively. Normally, these values can be obtained from the ratio of quasi-elastic broadenings along the two directions at the Brillouin zone boundary. However, within the measurements carried out at 80 K, where we achieve the best quasi-elastic signal, we see no sign of a difference between measurements along the ⟨100⟩ and ⟨110⟩ directions. We therefore suggest that the substrate potential appears to be isotropic. Further measurements with an improved intensity will be necessary to determine this point conclusively. Simulations show that small asymmetries (up to a few millielectronvolts) in the substrate potential have little effect on the resulting quasi-elastic broadening.

For the parameters above, an Arrhenius plot of the simulated broadenings yields an activation energy of $\sim 24 \pm 4$ meV. This is slightly lower than the experimental value of 31 ± 2 meV, yet higher than the potential corrugation. We find that the activation energy is almost independent of small changes in the barrier height. The fit to the experimental activation energy cannot be improved by varying the barrier height and friction, while still maintaining a fit to the momentum resolved data. It appears that activation of the diffusion is dominated by the local potential well created for each Cs atom by the strong interactions with its neighbours.

We are now in a position to summarize our new picture of the dynamics of Cs on Cu(001). At very low coverages (around 0.014 ML), motion is relatively weakly affected by Cs–Cs forces, since there is no evidence of de Gennes features in the experimental data. Under these conditions, the Cs behaves as almost independent particles, moving in a low friction regime with a significant fraction of long jumps. As the coverage is increased only slightly (e.g. to 0.044 ML), the inter Cs forces become much more important and dominate the dynamics. The de Gennes narrowing dip, and the increased quasi-elastic broadenings are consistent with the repulsive dipole–dipole interaction and dynamical motion between locations separated by a preferred length scale. Although the substrate potential corrugation is small, it provides an important modulation of the dynamics, effectively reducing the jump attempt rate and therefore reducing the quasi-elastic broadening magnitude to that observed.

6. Discussion

The established picture for Na adsorption on Cu(001) is that Na motion is strongly influenced by lateral forces from the substrate potential, but modulated by Na–Na interaction. In the case of Cs on Cu(001), the stronger Cs–Cs interactions can completely dominate the motion and lead to an acoustic vibration of the overlayer. However, the observation of quasi-elastic broadening under several different temperature and coverage conditions, along with the strong thermal damping of the Cs vibrational motion at low temperature, demonstrates the substrate corrugation also performs a crucial role in determining the behaviour of the system. By combining quasi-elastic and phonon information, we are able to develop a much more complete experimental picture.

Previous dynamical measurements on this system were not able to resolve the quasi-elastic broadening of Cs on Cu, and in fact this point was used to infer that Cs transport is much slower than we have now established experimentally. The acoustic phonon mode and its variation across the Na, K, Cs series (in fact its transition into a T-mode) have been measured and were reproduced within the mean field model proposed by Senet [20]. Here, the alkali interaction force was described by the sum of an adatom–substrate contribution and an adatom–adatom contribution. Within their model, the adatom–adatom contribution to the parallel vibration

energy is zero at the zone centre, and thus the vibration energy at the zone centre is a measure of the adatom–substrate interaction. Since the Cs phonon energy approaches zero at the zone centre, they concluded that the Cs vibrational motion is determined predominantly by the interlayer Cs–Cs interactions. Therefore the corrugation of the lateral substrate potential was negligible. Their model also implies that the curvature around the adsorption sites is negligible, so the T-mode frequency is vanishingly small.

Our measurements both support and provide considerably stronger evidence for the dominance of the Cs–Cs interaction, since we can identify and follow the acoustic mode towards zero energy transfer at lower momentum transfer values than are possible with time-of-flight techniques. However, we find the substrate corrugation is not negligible. Our analysis indicates that the phonon dispersion is not particularly sensitive to the amplitude of the substrate corrugation, particularly when the corrugation becomes comparable with the adsorbate thermal energies. Aperiodic dynamics, on the other hand, probe the entire surface potential and therefore quasi-elastic measurements are much more sensitive to the corrugation. Our MD simulations allow us to demonstrate that a potential of 20 ± 2 meV is necessary to reproduce the quasi-elastic measurements. We can therefore establish with some certainty that although the amplitude of the substrate potential is small, it must have a finite value.

It is informative to examine the results of MD simulations carried out with a flat potential, as these illustrate the qualitative differences between the proposed flat surface and experiment. Figure 7(a) shows the $S(\Delta\mathbf{K}, \omega)$ obtained using an almost flat potential (1 meV corrugation) and a low value of the friction ($\tau = 40$ ps), while figure 7(b) shows results for the same potential using a higher value of friction ($\tau = 2$ ps). In both cases, we see the results are qualitatively different from the experiment shown in figure 6(a). The combination of a flat potential and a low friction (figure 7(a)) reproduces the acoustic phonon structure at low $\Delta\mathbf{K}$, but the quasi-elastic peak shape is completely wrong. In particular, at large $\Delta\mathbf{K}$, the quasi-elastic mode is much too wide, i.e. the mobility is completely overestimated by this model. If we increase the friction in an attempt to reduce the quasi-elastic peak width, as shown in figure 7(b), we find that we can correct the quasi-elastic shape, but the acoustic phonon mode is lost. The damping of the vibrational mode can be understood intuitively, since the high friction leads to a thermalization of the Cs atom before it can complete one vibrational period. The only way to reproduce both the phonon and the correct quasi-elastic behaviour is to use a finite corrugation to slow down the rate of motion, accompanied by low friction in order to maintain the acoustic mode.

One of the other important observations is the disappearance of the Cs acoustic mode at low temperature and with decreasing coverage, both of which can be understood in terms of the competition between the Cs–Cs and Cs–Cu potentials and the affect of temperature. At low temperatures, the Cs atoms escape the substrate potential wells very infrequently. Consequently, the positions of the Cs atoms are quite restricted and the acoustic mode is disrupted. Similarly, at low coverages the large separations means the Cs–Cs forces are weak compared to the substrate forces and the acoustic mode is similarly disrupted. It is interesting to note that on the basis of this potential the simulations not only reproduce the acoustic phonon mode that we see in the experimental data, but at large momentum transfer they also predict the existence of an additional broad mode at an energy of about 1.2 meV. We attribute this to a true substrate T-mode. It is apparent over a range of coverages, and momentum transfers greater than about 1.5 Å^{-1}. Unfortunately, this is beyond the range which we can examine experimentally, so we cannot confirm this result explicitly. We can however, point out that the existence of a substrate corrugation means there must also be an associated T-mode, of some frequency. The suggestion of a T-mode energy of $\sim$1.2 meV is rather surprising, as we would normally expect the acoustic mode to show up as a modulation on top of the T-

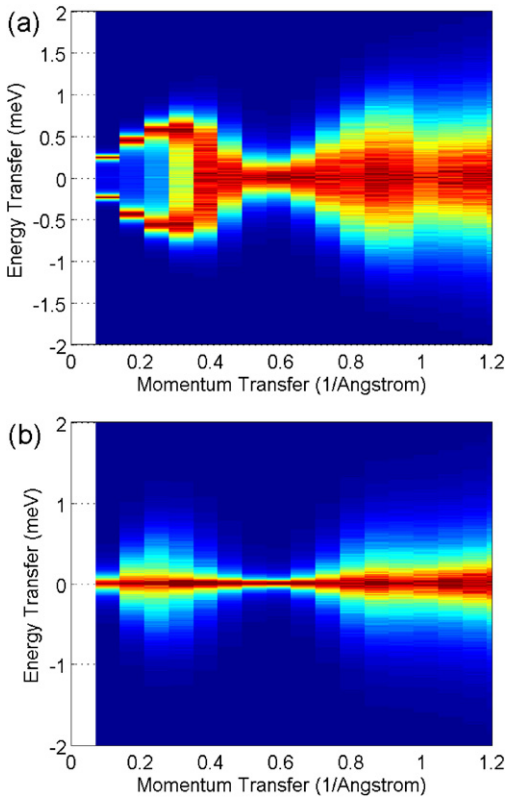

Figure 7. Langevin MD simulation of $S(\Delta\mathbf{K}, \omega)$ for Cs atoms at 130 K moving on an almost uncorrugated substrate potential (1 meV corrugation) with (a) an adsorbate–substrate friction parameter of $\eta = 1/40$ ps^{-1} and (b) an adsorbate–substrate friction of $\eta = 1/2$ ps^{-1}. The results have a qualitatively different shape to those seen experimentally and those obtained with the final simulation parameters; the qualitative 'arrowhead' shape is absent in these cases. The dramatic difference between these results and figure 6(a) illustrates the sensitivity of the $S(\Delta\mathbf{K}, \omega)$ to both the substrate corrugation and the friction.

mode, as described by Senet. In contrast, we clearly see the acoustic mode dispersing to zero, a value which is much lower than the T-mode energy. This discrepancy indicates the two modes are unexpectedly decoupled. We can understand the lack of coupling from the low friction regime of the system. Individual Cs atoms spend a fraction of their time in the substrate adsorption wells, where they oscillate with the T-mode frequency. During this time, we suggest interaction with neighbouring Cs atoms will yield a weak acoustic modulation on top of the T-mode frequency, although we cannot observe this in the experiment. Periodically, Cs atoms gain sufficient energy to leave the adsorption sites, either by energy transfer within the Cs overlayer or by thermal activation from the substrate. Once activated, the low friction regime of the system means they cannot lose energy quickly again, so spend an appreciable amount of time in an activated state, where they can move freely over the surface. Whilst activated, the Cs atoms predominantly ignore the substrate corrugation and explore the potential due to neighbouring Cs atoms, performing correlated motion and yielding the acoustic mode which disperses to zero. Overall, we again see that the characteristics of the system require strong interactions, a small but finite substrate corrugation, and low adsorbate–substrate friction. If any one of these three elements is altered, qualitatively different phenomenology is observed.

Table 1. Diffusion parameters for Na and Cs on (001). The two values of V_{xy} for Na correspond to the hollow bridge and the hollow top, respectively.

Parameter	Na	Cs
Arrhenius energy, E_a (meV)	58	31 ± 2
Potential corrugation, V_{xy} (meV)	75, 85	20 ± 2
Adsorbate–substrate friction (ps^{-1})	1/2	1/40

We now turn to the quality of our 2D Langevin MD model. Although the fit is not perfect, we reproduce all the main features of the data, including the changes with temperature and the development of the de Gennes features with coverage. The main discrepancies are that (i) the amplitude of the quasi-elastic broadenings at low momentum transfer is generally overestimated (figure 5(b)), (ii) the 0.014 ML measurements are slightly overestimated (figure 5(a)), while the 0.044 ML measurements at large $\Delta\mathbf{K}$ are slightly underestimated (figure 5(b)), and (iii) the simulated activation energy is slightly lower than the measured activation energy.

Clearly, for (i), the shape of the $\Delta E_{QE}/\Delta\mathbf{K}$ curve will be strongly affected by the Cs–Cs interaction model used. The dipole–dipole repulsion model used with Na–Cu(001) achieves a remarkable fit without empirical adjustment of the model parameters. However, in this case it appears that the model may require a small amount of additional refinement; for example altering the rate of decay of the interaction strength with distance. However, given the experimental uncertainties and the fact that the dipole–dipole model reproduces the main trends of the data set, we do not attempt to refine the interaction potential in order to improve the fit.

In terms of (ii), there is an indication that the friction may have a coverage dependence. For example, at low coverages the MD model overestimates the jump rate slightly (figure 5(a)) while, at higher coverages (figure 5(b)) the model underestimates the jump rate at high $\Delta\mathbf{K}$ values, where single-particle jumps dominate. Overall, the model cannot reproduce the entire data set perfectly with a single friction parameter suggesting that there may be an increase in friction with coverage. (Note that the simulation already incorporates energy transfer between Cs atoms through the Cs–Cs interaction model.)

Although we have determined a Cs–Cu(001) potential which is consistent with currently available experimental data, as is the usual case, we cannot guarantee it to be unique. In particular, the quantity of data available (limited by experimental signal) means that there are insufficient data at large momentum transfers for the detailed shape and isotropy of the potential to be examined. We note that varying the ratio E_t/E_b by about 20% does not produce significant changes in the simulated results, although raising or lowering the average potential does.

In the case of Na on Cu(001) we have recently observed an onset of vertical motion at coverages above about 0.05 ML [14]. The behaviour is characterized by a quasi-elastic broadening observed at $\Delta\mathbf{K} = 0$, which is only seen above a certain threshold coverage, but which increases above that threshold. The effect has been attributed to electronic charge rearrangement due to local density variations [36] and there is interest in exploring how widespread the phenomenon is. In the present set of Cs measurements, we do not see an increase in the quasi-elastic broadening at $\Delta\mathbf{K} = 0$ up to the maximum coverage we measured of about 0.06 ML. Thus, within the coverage range of our measurements there is no indication of perpendicular motion of the Cs atoms.

Table 1 summarizes and compares the diffusion parameters for Na and Cs on Cu(001). Both the Arrhenius energy and the potential corrugation for Cs are lower than for Na. It is

interesting to note that unlike the usual trend, the potential corrugation in the case of Cs is smaller than the Arrhenius activation energy. We attribute this to the strong Cs–Cs interactions compared to the strength of the Cs–substrate potential.

7. Conclusions

We have made ^{3}He spin-echo measurements of the dynamics of Cs on Cu(001), observing for the first time quasi-elastic broadening and simultaneous phonon dispersion. Unlike in all other ^{3}He spin-echo studies to date, the mixed phonon and quasi-elastic components necessitated energy domain analysis in order to separate the two contributions. Our results demonstrate that although the Cs dynamics are dominated by Cs–Cs repulsion as expected, the repulsion does not impede movement. Cs transport proceeds by rapid jumping between locations, while maintaining a characteristic adsorbate separation that is dictated by the strong Cs–Cs repulsion.

Langevin molecular dynamics simulations using a dipole–dipole repulsion model for the inter Cs forces reproduce the main trends of the experimental data set when combined with an adsorbate–substrate potential corrugation of 20 ± 2 meV and a constant adsorbate–substrate friction of $1/40$ ps^{-1}. These results are in contrast to earlier models which suggested a virtually uncorrugated substrate potential. Overall, the effects of the Cs–Cs potential, the Cs–substrate potential, adsorbate–substrate friction and temperature give rise to the complex behaviour of the quasi-elastic and phonon modes. In particular, we see that quasi-elastic measurements provide a particularly sensitive probe of the substrate potential.

At coverages of up to 0.06 ML we see no evidence for the perpendicular motion recently observed in the case of Na/Cu(001). However, there is some evidence that the friction may increase with coverage and, unlike for Na/Cu(001), the dipole–dipole model may require some refinement in order to fully reproduce the Cs/Cu(001) data.

Acknowledgments

APJ is grateful for a University Research Fellowship from the Royal Society. GA is grateful for a research fellowship from Gonville & Caius College Cambridge and RDD support from the Fulbright Foundation.

References

[1] Langmuir I and Kingdon K H 1923 *Science* **57** 58
[2] Gurney R W 1935 *Phys. Rev.* **47** 479
[3] Schmalz A, Aminpirooz S, Becker L, Haase J, Neugebauer J, Scheffler M, Adams D L and Bøgh E 1991 *Phys. Rev. Lett.* **67** 2163
[4] Over H, Bludau H, Skottke-Klein M, Ertl G, Moritz W and Campbell C T 1992 *Phys. Rev.* B **45** 8638
[5] Fisher D, Chandavarkar S, Collins I R, Diehl R D, Kaukasoina P and Lindroos M 1992 *Phys. Rev. Lett.* **68** 2786
[6] Andersen J N, Lundgren E, Nyholm R and Qvarford M 1993 *Surf. Sci.* **289** 307
[7] Neugebauer J and Scheffler M 1992 *Phys. Rev.* B **46** 16067
[8] Stampfl C, Scheffler M, Over H, Burchhardt J, Nielsen M M, Adams D L and Moritz W 1992 *Phys. Rev. Lett.* **69** 1532
[9] Neugebauer J and Scheffler M 1994 *Prog. Surf. Sci.* **46** 295
[10] Stampfl C, Neugebauer J and Scheffler M 1994 *Surf. Sci.* **307–309** 8
[11] Diehl R D and McGrath R 1996 *Surf. Sci. Rep.* **23** 43
[12] Diehl R D and McGrath R 1997 *J. Phys.: Condens. Matter* **9** 951
[13] Graham A P 2003 *Surf. Sci. Rep.* **49** 115
[14] Alexandrowicz G, Jardine A P, Hedgeland H, Allison W and Ellis J 2006 *Phys. Rev. Lett.* **97** 156103
[15] Cousty J, Riwan R and Soukiassian P 1985 *Surf. Sci.* **152/153** 297

[16] Witte G 2004 *J. Phys.: Condens. Matter* **16** S2937–52
[17] Meyerheim H L, Wever J, Jahns V, Moritz W, Eng P J and Robinson I K 1994 *Surf. Sci.* **304** 267
[18] Meyerheim H L, Wever J, Jahns V, Moritz W, Eng P J and Robinson I K 1994 *Physica* B **198** 66
[19] Meyerheim H L, Moritz W, Schultz H, Eng P J and Robinson I K 1995 *Surf. Sci.* **331–333** 1422
[20] Senet P, Toennies J P and Witte G 1999 *Chem. Phys. Lett.* **299** 389
[21] Witte G and Toennies J P 2000 *Phys. Rev.* B **62** R7771
[22] Persson B N J and Ryberg R 1985 *Phys. Rev.* B **32** 3586
[23] Jardine A P, Dworski S, Fouquet P, Alexandrowicz G, Riley D J, Lee G Y H, Ellis J and Allison W 2004 *Science* **304** 1790
[24] Fouquet P, Jardine A P, Dworski S, Alexandrowicz G, Allison W and Ellis J 2005 *Rev. Sci. Instrum.* **76** 053109
[25] Alexandrowicz G and Jardine A P 2007 *J. Phys.: Condens. Matter* **19** 305001
[26] Jardine A P, Ellis J and Allison W 2002 *J. Phys.: Condens. Matter* **14** 6173
[27] Mezei F 1980 *Neutron Spin Echo* (*Springer Lecture Notes in Physics*) (Berlin: Springer)
[28] Van Hove L 1954 *Phys. Rev.* **95** 249
[29] Fouquet P and Witte G 1999 *Phys. Rev. Lett.* **83** 360
[30] Ellis J, Graham A P, Hofmann F and Toennies J P 2001 *Phys. Rev.* B **63** 195408
[31] Hedgeland H 2006 *PhD Thesis* University of Cambridge
[32] de Gennes P G 1959 *Physica* **25** 825
[33] Jardine A P, Ellis J and Allison W 2004 *J. Chem. Phys.* **120** 8724
[34] Graham A P, Hofmann F, Toennies J P, Chen L Y and Ying S C 1997 *Phys. Rev. Lett.* **78** 3900
[35] Arena D A, Curti F G and Bartynski R A 1997 *Phys. Rev.* B **56** 15404
[36] Fratesi G *et al* 2007 to be published